Chemical Vapor Deposition

DOI: 10.1002/cvde.200906778

Full Paper

In-Situ Growth and Characterization of Highly Textured $La_{0.9}Sr_{0.1}MnO_3$ Films on $LaAlO_3(100)$ Substrates**

By *Roberta G. Toro*,* *Graziella Malandrino*,* *Laura M.S. Perdicaro*, *Davide M.R. Fiorito*, *Antonello Andreone*, *Gianrico Lamura*, and *Ignazio L. Fragalà*

$La_{0.9}Sr_{0.1}MnO_3$ (LSMO) films are grown on $LaAlO_3(100)$ substrates through metal-organic (MO)CVD using ''second generation'' precursors of Sr, La, and Mn. An in-situ novel MOCVD strategy is adopted which involves the use of two different molten mixtures consisting of the $La(hfa)_3$•diglyme and $Sr(hfa)_2$•tetraglyme adducts as La and Sr sources, respectively, and $Mn(hfa)_2$•tmeda or $Mn(tmhd)_3$ as Mn precursor [Hhfa = 1,1,1,5,5,5-hexafluoro-2,4-pentanedione, diglyme = bis(2-methoxyethyl)ether, tetraglyme = 2,5,8,11,14-pentaoxapentadecane, tmeda = N,N,N′,N′-tetramethylethylendiamine and H-tmhd = 2,2,6,6-tetramethyl-3,5-heptandione]. The X-ray diffraction (XRD) patterns show that the films are *c*-axis oriented. Pole figures are applied as a simple non-invasive tool to assess the textural nature of these LSMO films. The morphology is investigated using the scanning electron microscopy (SEM) and atomic force microscopy (AFM) that reveal the presence of grains, 300 nm average dimensions, and a root mean square (rms) surface roughness of 21 nm. Chemical composition through energy-dispersive X-ray (EDX) analysis indicates that the films possess a stoichiometry of about 0.9:0.1:1 ratio, while X-ray photoelectron spectroscopy (XPS) depth profiles are used to assess the vertical compositional homogeneity. The ferromagnetic/paramagnetic and metallic/insulating transition temperatures are determined by standard four-contact resistivity versus temperature measurements.

Keywords: Manganites, Transport properties, Multicomponent source, Depth profile, Texture

1. Introduction

Recently, the strontium-doped lanthanum manganite materials, $La_{1-x}Sr_xMnO_3$, have been the subject of extensive studies because of their intriguing electrical and magnetic properties which render them potential candidates for many practical applications. Considering the chemical stability, thermal expansion match, and electrical conductivity, for example, $La_{1-x}Sr_xMnO_3$ is the most commonly used electrode material in solid oxide fuel cells (SOFCs).[1] In this context, much of the experimental work has focused on polycrystalline compounds to be used as cathodes in SOFCs.

In addition, another very interesting property of these doped manganite perovskite materials is the colossal magneto-resistance (CMR) phenomenon around the ferromagnetic transition temperature (T_C), which consists of the dramatic decrease of their resistance (negative magneto-resistance) when an external magnetic field is applied. For this reason the manganite films have been proposed as active components in non-volatile magnetic random access memory,[2] magneto-resistive read-head,[3] and semiconductor field effect transistors.[4] This particular behavior was earlier explained by the theory of double exchange (DE),[5] for which the Mn ions can exchange their valence by simultaneous jump of the e_g electrons of Mn^{3+} on the empty e_g orbital of Mn^{4+} through the O p-orbital. Moreover, in the presence of an external magnetic field, adjacent Mn ions have their spins perfectly aligned. This new situation allows an easier electron transfer from one Mn ion to another, causing a net decrease of resistance.[6] It has also been shown that small alterations in the perovskite unit cell, such as Mn-O bond length d or Mn-O-Mn bond angle θ, induce dramatic effects in the physical properties of the bulk material. Epitaxial strain, due to the lattice mismatch between the film and the substrate, is expected to play an important role in determining magnetic and electrical properties such as the temperature and field behavior of the resistivity, the ferromagnetic transition temperature T_c, and the metallic/insulating transition temperature T_P.[7,8]

Since most of the technological applications require the synthesis of high-quality epitaxial $La_{1-x}Sr_xMnO_3$ thin films,[9] the study of their structural properties as a function

[*] Dr. R. G. Toro, Prof. G. Malandrino, Prof. I. L. Fragalà, Dr. L. M. S. Perdicaro, D. M. R. Fiorito
Dipartimento di Scienze Chimiche, Università di Catania, ISTM-CNR and INSTM, UdR Catania V.le Andrea Doria 6, 95125 Catania, (Italy)
E-mail: rgtoro@unict.it; gmalandrino@dipchi.unict.it
Prof. A. Andreone, Dr. G. Lamura
CNR-INFM Coherentia and CNISM-Department of Physics, University of Naples Federico II Piazzale Tecchio 80, 80125, Napoli, (Italy)

[**] The authors thank the MIUR for the financial support within the FISR thematic activities: Nanosystems of transition metal oxide for solid oxide fuel cells (SOFCs) (New systems for energy production and storage program).

of the synthetic procedure is of crucial interest from both fundamental and applicative points of view.

At the same time developing a ''user friendly'' and low-cost route to this material in the form of thin film represents a challenging goal. In fact, the ability to produce high-quality $La_{1-x}Sr_xMnO_3$ thin films deposited through an industrially transferable and scalable methodology is necessary for introducing $La_{1-x}Sr_xMnO_3$ into electronic and magnetic devices. MOCVD has the potential advantage of being a very reliable and reproducible method for the fast production of films with a high degree of uniformity in both thickness and composition over large areas.[10] Conventional MOCVD processes have already been tested as a synthetic route to the fabrication of $La_{1-x}Sr_xMnO_3$ films showing very great magneto-resistance properties.[11–13] Nevertheless, a synthetic approach able to selectively deposit films with a defined stoichiometry is crucial since the CMR effect is strictly related to the Sr doping amount. In particular, $La_{0.9}Sr_{0.1}MnO_3$ films have not to date been deposited by MOCVD, and at the same time it has been reported that LMSO films show, under particular conditions, a metallic to insulating transition at higher than room temperatures.[14] In addition, a well-defined stoichiometry is also a crucial issue for applications of LSMO as the cathode in thin films SOFCs. In regard to deposition rates and film porosity, other important issues for potential SOFC applications, MOCVD represents one of the most promising routes to the deposition of films for intermediate temperature micro SOFCs. In this context, physical vapor deposition (PVD) techniques may present drawbacks associated with low deposition rates, in some cases, and/or difficulty in controlling the film porosity. On the other hand, chemical approaches such as solution routes may present difficulties in controlling accurately, in a reproducible manner, the stoichiometry of complex oxides.

In this paper, we report on a very simple, low-cost strategy for the deposition of LSMO *c*-axis oriented films on $LaAlO_3(100)$ substrates through an in-situ MOCVD process. The aim of this study is to develop a new synthetic strategy using a multi-component source approach, which may be used as a simple route to the fabrication of layers to be used as cathodes in SOFCs. Two different La-Sr-Mn precursor sources have been applied that consist of the $La(hfa)_3$•diglyme and $Sr(hfa)_2$•tetraglyme precursors in mixture with the $Mn(tmhd)_3$ β-diketonate or alternatively with the $Mn(hfa)_2$•tmeda adduct [H-hfa = 1,1,1,5,5,5-hexafluoro-2,4-pentandione; H-tmhd = 2,2,6,6-tetramethyl-3,5-heptandione, diglyme = $CH_3O(CH_2CH_2O)_2CH_3$); tetraglyme = 2,5,8,11,14-pentaoxapentadecane; tmeda = N,N,N′,N′-tetramethylethylendiamine]. Both multi-element mixtures have been used to deposit LSMO thin films on $LaAlO_3(100)$ substrates. In particular, the relationship among structural characteristics/compositional homogeneity and the applied multicomponent mixture has been investigated and discussed. Morphological properties of thin films have been investigated through SEM and AFM. Structural information and the lattice parameters have been determined using XRD, while the composition has been analyzed through EDX. Resistivity has been measured by the standard four-probe method revealing transport and magnetic properties better than those of the bulk samples. Finally, the present approach has been adopted to deposit LSMO films on yttria stabilized zirconia (YSZ) pellets.

2. Results and Discussion

2.1. Thermal Analysis of the Precursor Mixtures

The present MOCVD process relies upon a novel approach based on the use of multi-component ''single'' sources. A similar approach has been successfully applied for a large variety of thin film materials ranging from $LaAlO_3$,[15] $La_{2-x}Ba_xOCuO_{4+\delta}$,[16] BaCaCuOF matrices for $Tl_2Ba_2CaCu_2O_x$ films,[17] $YBa_2Cu_3O_{7-\delta}$[18] and $CaCu_3Ti_4O_{12}$[19] films.

The second generation $Mn(hfa)_2$•tmeda precursor is stable in air and shows a low melting temperature (69–73 °C) that renders the precursor a liquid source with constant surface area and vapor pressure at operating temperatures. Details of synthetic procedure, X-ray single-crystal structure, and complete physico-chemical characterization have been reported elsewhere.[20]

The thermogravimetric (TG) profiles of $Mn(hfa)_2$•tmeda and $Mn(tmhd)_3$ show a single step, that may be associated with vaporization without any decomposition process. Trends of TG atmospheric pressure vaporization rates vs. temperature of $Mn(hfa)_2$•tmeda and $Mn(tmhd)_3$ complexes are compared to those of $La(hfa)_3$•diglyme and $Sr(hfa)_2$•tetraglyme (Fig. 1). It becomes evident that the molten $Mn(hfa)_2$•tmeda adduct is much more volatile than the ''first generation'' $Mn(tmhd)_3$ solid complex. All the

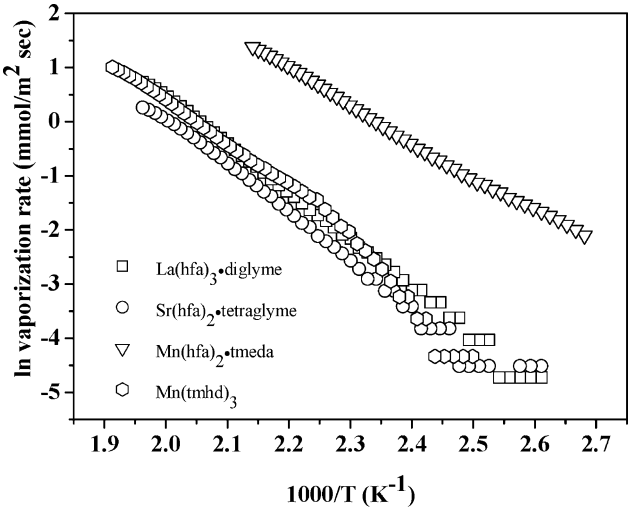

Fig. 1. Atmospheric pressure TG vaporization rate data of adducts La(hfa)$_3$•diglyme, Sr(hfa)$_2$•tetraglyme, Mn(hfa)$_2$•tmeda, and Mn(tmhd)3 as a function of inverse temperature.

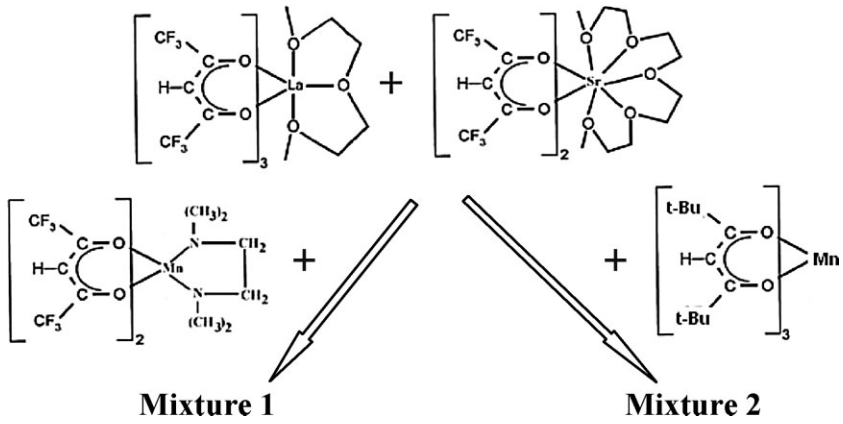

Scheme 1. The La-Sr-Mn precursor mixtures involved in the MOCVD process.

complexes show a linear behavior of the vaporization rate, a clear indication that no secondary phenomena, such as decomposition, accompany the evaporation process.

The $Mn(hfa)_2$•tmeda and $Mn(tmhd)_3$ precursors have been applied as Mn sources in two different mixtures (Scheme 1). In particular, the $La(hfa)_3$•diglyme, $Sr(hfa)_2$•tetraglyme, and $Mn(hfa)_2$•tmeda (mixture 1) are mixed in a stoichiometric 0.37:0.07:0.17 mole ratio thus yielding a molten source of La, Sr, and Mn. In the case of the $La(hfa)_3$•diglyme, $Sr(hfa)_2$•tetraglyme, and $Mn(tmhd)_3$ (mixture 2) the ratio used is 0.75:0.20:0.50. In both cases, $La(hfa)_3$•diglyme acts as a solvent for the Sr and Mn precursors, as previously reported for the case of $LaAlO_3$ film growth.[15,16]

Evaporation from the molten sources has been achieved at a constant temperature of 110 °C and 130 °C for mixtures 1 and 2, respectively. The use of fluorinated sources, i.e., the presence of fluorine in the Sr, Mn, and La architectural frameworks, has required an accurate optimization of MOCVD parameters and the use of water vapor-saturated oxygen flow to obtain fluorine-free films (vide infra).

2.2. MOCVD LSMO Films From Mixtures 1 and 2

LSMO films have been deposited from a molten multi-component precursor source on $LaAlO_3$(100) substrates at deposition temperatures ranging from 750 to 1000 °C.

LSMO has a distorted perovskite-like structure with an orthorhombic Pbnm symmetry having lattice parameters at room temperature of $a = 0.5547$ nm, $b = 0.5560$ nm, and $c = 0.7736$ nm.[21] On the other hand, LSMO grown on $LaAlO_3$ substrates can be considered as a pseudocubic structure the lattice parameters of which are $a_c = a/\sqrt{2}$, $b_c = b/\sqrt{2}$, and $c_c = c/2$.[21] Note that the $LaAlO_3$ substrate also has a perovskite structure, the unit cell of which can be described as pseudocubic (lattice constant $a = 0.379$ nm), even though the system has a 0.2% rhombohedral (r) distortion. Thus, the pseudocubic indexing will be used, in the following, for both systems. In this context, the $LaAlO_3$ substrate lattice parameter is only 0.014 nm smaller than a_c for LSMO and, therefore, it represents a suitable substrate for film growth. The MgO substrates have been used to accurately determine the film composition, avoiding the contribution of La deriving from the substrate.

The nature of fabricated LSMO has been investigated by XRD. The XRD studies performed on films deposited at lower temperatures from mixture 1, i.e., below 900 °C, point to the formation of strontium fluoride, SrF_2, together with the formation of the LSMO polycrystalline phase. In fact, the XRD pattern of a sample deposited at 850 °C (Fig. 2) shows the presence of peaks related to the LSMO phase in addition to the peaks at $2\theta = 26.3°$, 30.3°, 43.9°, 52.01° associated with the SrF_2 111, 200, 220, and 311 reflections, respectively.

Deposition temperatures higher than 900 °C provide films consisting of a pure LSMO phase, and no peaks of fluoride phases are observed in the pattern. A typical XRD θ-2θ scan of a film deposited at 1000 °C (Fig. 3a) shows only two

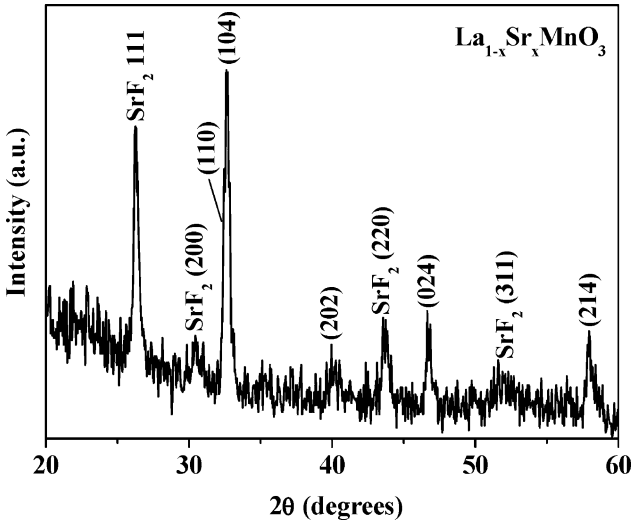

Fig. 2. XRD pattern of a polycrystalline $La_{1-x}Sr_xMnO_3$ film deposited at 850 °C from mixture 1.

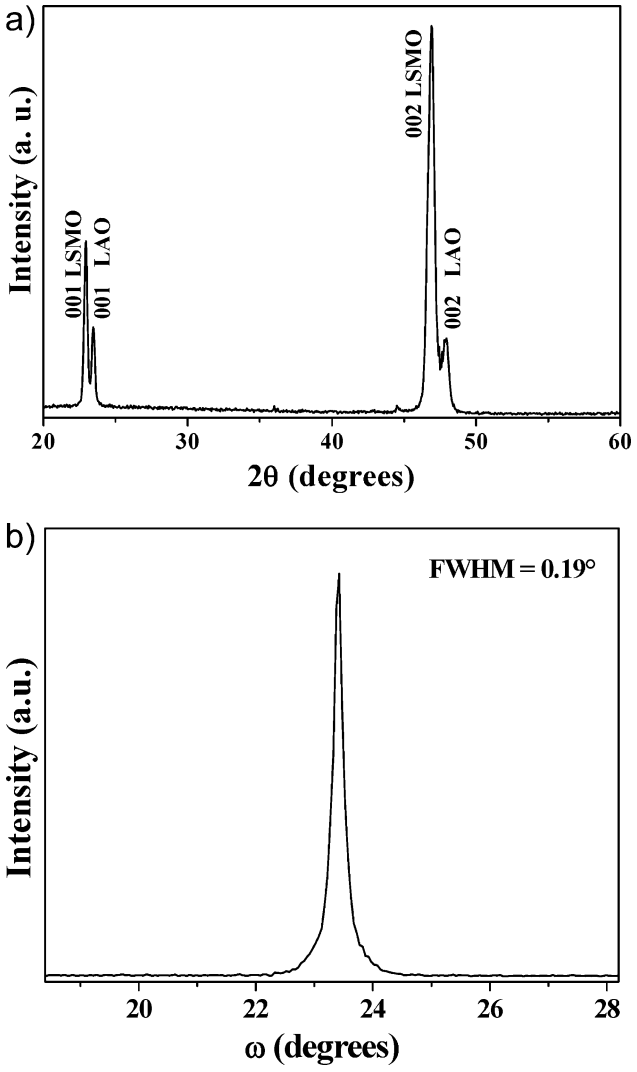

Fig. 3. a) XRD pattern of a c-axis oriented $La_{0.93}Sr_{0.13}MnO_3$ film deposited at 1000 °C from mixture 1. b) Rocking curve of the 002 reflection.

reflection peaks at $2\theta = 22.95°$ and $2\theta = 46.90°$ corresponding, respectively, to the 001 and 002 reflections of the LSMO phase, in addition to the 001 and 002 reflections of the $LaAlO_3$ substrate. The unique presence of the (00ℓ) reflections clearly indicates that LSMO films are preferentially *c*-axis-oriented with respect to the substrate. In fact the *d* values of the LSMO phase are compatible with a *c*-axis growth since the lattice parameter, determined considering the position of the 00ℓ peaks, is 0.3871 ± 0.0004 nm. This value agrees quite well with the c_c axis constant of the pseudocubic cell ($c_c = 0.3868$ nm). Note that the a_c and b_c lattice constant values are 0.3922 and 0.3931 nm, respectively. The absence of any other peaks in the pattern confirms that no other detectable phases are formed when films are deposited at higher temperatures. To confirm the out-of-plane alignment the rocking curve of the 002 reflection has been measured and is reported in Figure 3b. The rocking curve shows a full width at half maximum (FWHM) value of 0.19°, which indicates a low dispersion of grains, i.e., grains have a good out-of-plane alignment.

The in-plane alignment has been studied by recording pole figures of the oriented films. Four poles are observed at $\Psi = 45°$ every 90° of φ (Fig. 4) for the 011 pole, as expected for a pseudocubic symmetry. This is indicative of a good in-plane alignment of grains vs. the substrate.

There is, therefore, indication from XRD measurements, that (00ℓ)-textured LSMO films have been grown on $LaAlO_3(001)$ with a typical cube-on-cube growth, involving one LSMO unit cell matching one $LaAlO_3(100)$ unit cell. Their epitaxial relationships can be summarized as follows: $(001)LaAlO_3||(001)LSMO$ $\langle 100\rangle LaAlO_3||\langle 100\rangle LSMO$. Quite similar structural data have been obtained for LSMO samples deposited from mixture 2.

The surface morphology of LSMO films has been imaged by SEM. The in-situ-grown LSMO films (mixture 1) have smooth and homogeneous surfaces (Fig. 5a) with cube-like grains. The grain dimensions are determined to be about 300 nm. A SEM image of the cross-section (Fig. 5b) shows that films possess a typical columnar growth. The thickness of these films is about 2 μm. The surface roughness of films has been investigated using AFM (Fig. 6). The rms roughness of the film surface measured on a 3.0 μm × 3.0 μm m area is 21 nm. LSMO films grown from mixture 2 have a similar morphology with well-defined cubic grains having an average dimension of about 200 nm (Fig. 5c).

The film composition has been determined by EDX. The quantitative EDX analyses of LSMO films deposited at 1000 °C from both mixtures have been carried out on samples deposited on MgO, due to the overlap of the La signals coming from the film and the substrate.

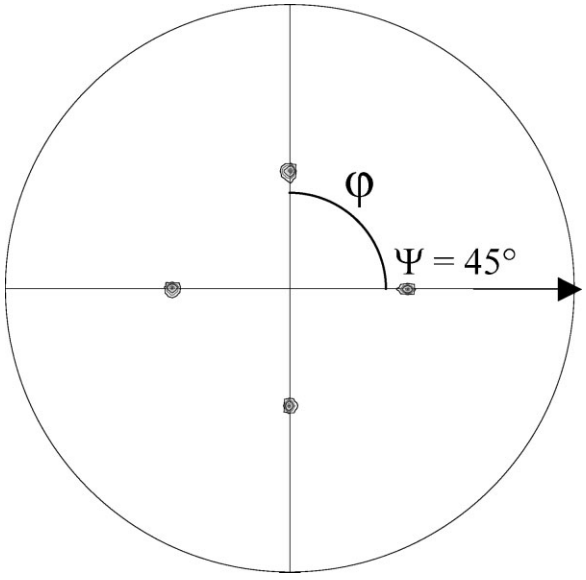

Fig. 4. The 011 ($2\theta = 32.31°$) pole figure of the $La_{0.93}Sr_{0.13}MnO_3$ film deposited at 1000 °C on $LaAlO_3(001)$ from mixture 1.

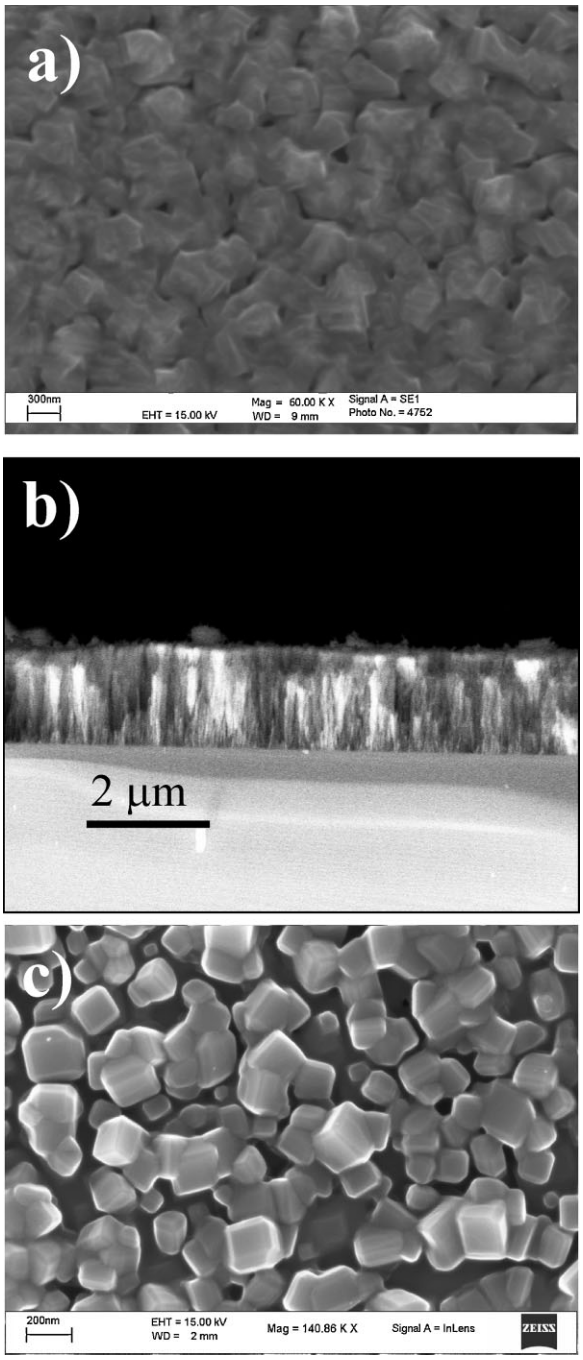

Fig. 5. SEM images of a) the LSMO film surface (mixture 1), and b) the film cross-section. c) SEM image of the LSMO film grown from mixture 2.

The analyses carried out on several selected areas indicate that the La/Sr/Mn ratio of the film is $0.93 \pm 0.04{:}0.13 \pm 0.03{:}1.00 \pm 0.05$ over the whole $10\,\text{mm} \times 10\,\text{mm}$ surface. The La L lines are spread in the 4.500–5.850 keV range, the Sr L and O K_α peaks are found at 1.800–1.900 and 0.520 keV, respectively, while the Mn K_α, K_β and L peaks are observed at 5.887, 6.496 and 0.637 keV, respectively (Fig. 7). The substrate peak is found at 1.253 keV (Mg K_α). In addition, EDX data rule out the presence of contaminant elements such as C or F. Similar data have been obtained for LSMO films deposited from mixture 2. The observed difference between thin film stoichiometry and the stoichiometry of the precursor mixture may be more likely to be related to the vaporization step than to different deposition behaviors of the precursors.

The resistance vs. temperature plot for a LSMO film deposited from mixture 1 on the $LaAlO_3$ substrate at 1000 °C is shown in Figure 8. Two different directions for the excitation current have been probed revealing the same general temperature behavior but different high temperature resistivity values. The resistivity is metallic below its corresponding T_P and it is insulating above T_P. The ferromagnetic to paramagnetic (FP) transition temperature T_C (Curie temperature) and the metallic to insulating (MI) transition have been evaluated by taking the inflection point and the maximum of the $\rho(T)$ curve, respectively. $T_C = 269\,\text{K}$ (±1%), $T_P = 287\,\text{K}$ (±1%) and $T_C = 260\,\text{K}$ (±1%), $T_P = 280\,\text{K}$ (±1%) have been obtained for the two directions. The magneto-resistance properties have been extensively studied for LSMO films, but it is interesting to note that present values of T_P and T_C are higher than those reported for $La_{1-x}Sr_xMnO_3$ single crystals with similar doping levels ($T_P = 145\,\text{K}$ for $x = 0.1$ and $T_P = 238\,\text{K}$ for $x = 0.15$).[14,22] In addition, they compare well with T_P values observed for thin films grown by pulsed laser ablation, molecular beam epitaxy, and sputtering on different substrates.[23] The slightly different values both in terms of transport and magnetic properties may be due to the compositional gradient and/or to the presence of grain boundaries.

To this aim, i.e., to assess the vertical homogeneity of the two types of samples, XPS depth profile analyses were carried out on LSMO samples deposited on MgO substrates. The XPS analyses confirm the absence of any contaminants through the deposited layers. The XPS profile of the LSMO sample deposited from mixture 1 (Fig. 9a) shows a non-homogeneous distribution of La and Mn along the film thickness. These results may be explained considering that the La(hfa)$_3$•diglyme/Sr(hfa)$_2$•tetraglyme/Mn(hfa)$_2$•tmeda mixture does not permit control of the different sublimation rates of the three precursors, and causes the variation of chemical composition along the film thickness. In fact, the Mn precursor is more volatile thus it is likely that, at the beginning of the deposition, source vapors are richer in Mn. During the film growth, the source vapors become progressively poorer in Mn precursor, thus the LSMO films show a chemical gradient from the interface toward the surface.

On the other hand, note that the XPS results for the sample deposited from mixture 2 (Fig. 9b) confirm that the La/Sr/Mn/O atomic ratios remain constant along the entire film thickness. These data indicate that the use of the La(hfa)$_3$•diglyme/Sr(hfa)$_2$•tetraglyme/Mn(tmhd)$_3$ mix-

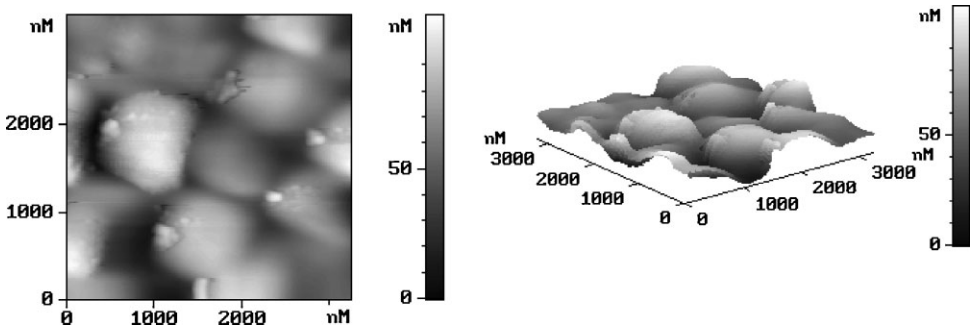

Fig. 6. AFM image of the LSMO film deposited from mixture 1 at 1000 °C on $LaAlO_3$(001).

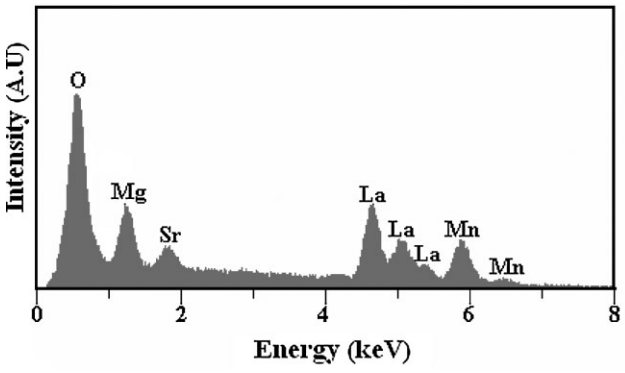

Fig. 7. EDX spectrum of a LSMO film deposited on MgO substrate from mixture 1.

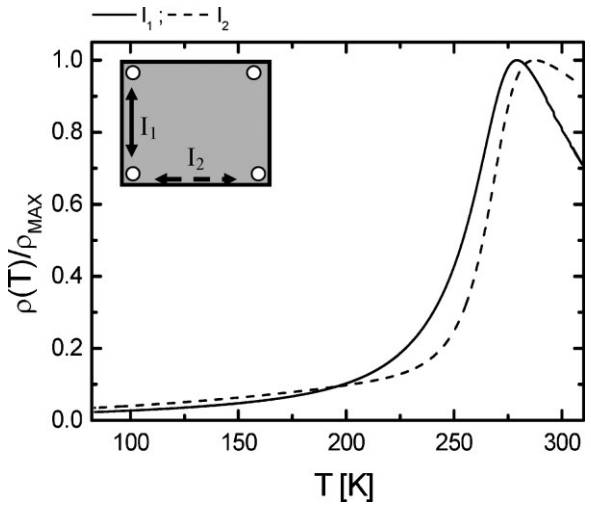

Fig. 8. Normalized resistivity of the $La_{0.93}Sr_{0.13}MnO_3$ film deposited from mixture 1 on $LaAlO_3$(001) substrate at 1000 °C as a function of the temperature. Two different run data (the continuous and dashed lines) were taken by injecting the current following directions 1 and 2 respectively as represented in the inset.

ture allows a more precise control of the vaporization rates of all the elements, thus avoiding the formation of a chemical gradient through the film thickness. Since mixture 2 is proven to produce homogeneous films on single crystal substrates, it has been applied to the deposition of the LSMO films on pellets of YSZ, to date the most used electrolyte in SOFCs. The XRD pattern of the film deposited from mixture 2, using the same conditions above reported for the deposition on single crystal substrates, shows the presence of all the reflections of the LSMO phase (ICDD N°47-444) (Fig. 10).

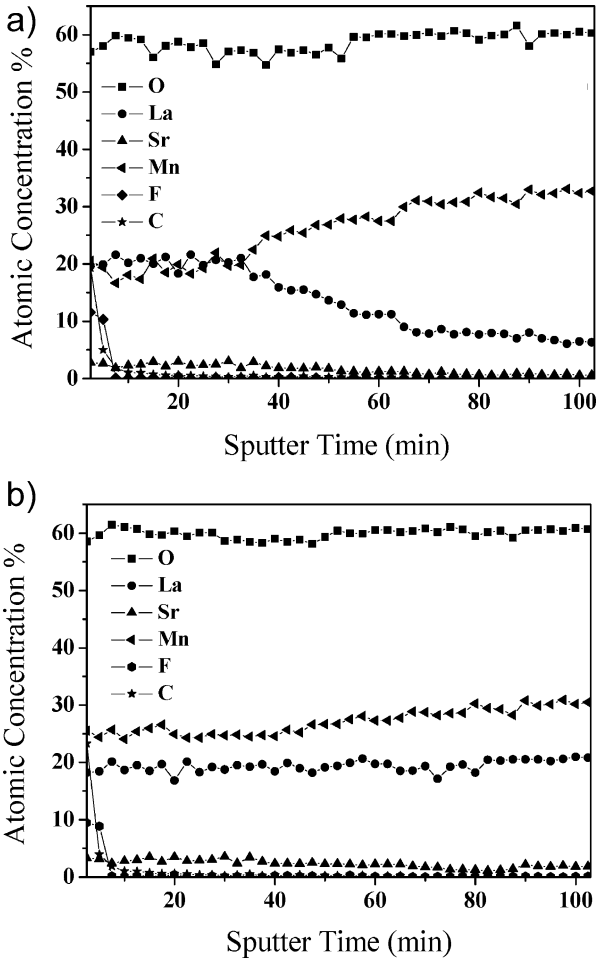

Fig. 9. XPS depth profiles of films deposited on MgO substrates: a) LSMO sample obtained from mixture 1 and b) from mixture 2.

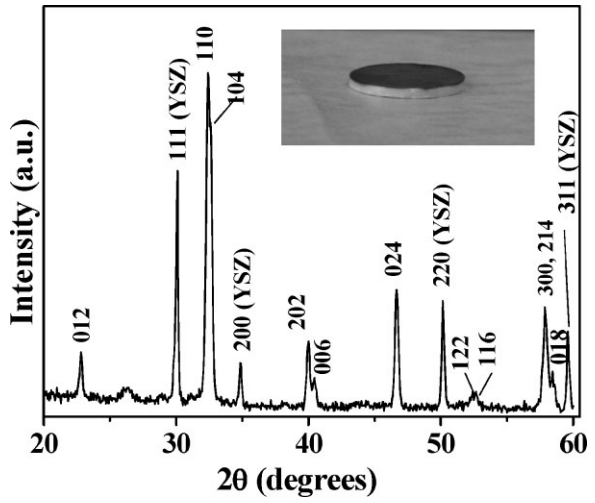

Fig. 10. XRD pattern of a polycrystalline LSMO film deposited from mixture 2 on the YSZ pellet (see inset).

3. Conclusions

In summary, the in-situ MOCVD growth of LSMO films using a molten, multimetal source has been achieved. It has been demonstrated that LSMO thin films can be grown using two different Mn precursors, namely $Mn(hfa)_2$•tmeda or $Mn(tmhd)_3$, in mixtures with the La and Sr sources, thus obtaining two different La-Sr-Mn precursor mixtures. The novelty of the present study relies upon the use of a molten precursor mixture approach that represents an interesting and convenient alternative to the adoption of different sources for each component since, of course, this would require the control of different parameters (gas flows and sublimation temperatures) for each source. The in-situ deposited LSMO(001) films on $LaAlO_3$(001) substrates are of high quality as demonstrated by their in-plane and out-of-plane alignments investigated using XRD measurements. It has been shown that the $Mn(tmhd)_3/La(hfa)_3$•diglyme/ $Sr(hfa)_2$•tetraglyme mixture produces films with better vertical compositional homogeneity of the deposited layer. Present data indicate that this approach has the advantage of being a very simple method for the easy production of lanthanum manganites on large areas.

Finally, the values of FP and MI transition temperatures confirm that the reported MOCVD route represents a promising approach to the fabrication of high-quality LSMO films.

4. Experimental

Precursors and Characterization: The $La(hfa)_3$•diglyme, $Sr(hfa)_2$• tetraglyme, and $Mn(hfa)_2$•tmeda were synthesized as described elsewhere [20,24]. $Mn(tmhd)_3$ complex was purchased from Strem Chemicals and used without further purification. TG measurements were made using a Mettler Toledo TGA/SDTA 851^e. Analyses were made under pre-purified nitrogen using a 5 °C min^{-1} heating rate. Temperature was measured with an accuracy of ±0.1 °C.

MOCVD of $La_{1-x}Sr_xMnO_3$: Thin film depositions were performed in a horizontal, low-pressure, hot-wall MOCVD reactor. Precursor mixtures 1 and 2 were heated at 110 °C and 130 °C, respectively, which represent suitable temperatures for the efficient vaporization without thermal degradation for the two mixtures. Argon was used as a carrier gas (flow = 200 sccm), while the reactant gas (oxygen/water vapor mixture, flow = 900 sccm) was introduced into the main flow in the vicinity of the reaction zone. In order to introduce H_2O vapors into the reaction atmosphere, oxygen was bubbled through a distilled water reservoir kept at room temperature. The gas flows were controlled by mass flowmeters and the total pressure was held at 12.0 Torr (background pressure = 0.10 Torr). In each case the deposition time was 120 min and the mass of weighed precursor was 450 mg. (100)$LaAlO_3$ and (100)MgO substrates were used. Depositions were carried out in the range 750–1000 °C.

Film Characterization: Film atomic composition was determined by EDX analysis, using an Oxford solid state detector, and XPS analysis, using a Phi ESCA/SAM 5600 Multy technique spectrometer. A standard Al Kα radiation source ($h\nu$ = 1486.0 eV) was used. Depth profiles were obtained by alternating sputter etching rastered over a 4 mm × 4 mm area (with a 4 kV argon-ion gun) and XPS analysis.

Morphologies were examined through SEM, using a LEO Iridium 1450 microscope. Structures of crystalline phases and in-plane and out-of-plane alignments were studied through accurate XRD measurements. θ-2θ XRD patterns were recorded using a θ-θ Bruker D5005 diffractometer using Cu Kα radiation at 30 mA and 40 kV, and a scan step of 0.05°. Pole figures were recorded on a θ-2θ Bruker D5005 diffractometer equipped with an Eulerian cradle.

The measurement of the temperature dependence of resistivity in zero magnetic field was performed in the standard four-probe configuration, with the usual compensation of thermoelectric bias by inversion of the direction of current flow. Electrical contacts to the samples were provided by direct silver paste soldering on the manganite film. The contact area never exceeded 1 mm^2.

Received: January 13, 2009
Revised: February 24, 2010

[1] R. Ruffo, C. M. Mari, V. Migani, I. Natali Sora, *Ionics* **2008**, *14*, 107.
[2] Y. Lu, X. W. Li, G. Q. Gong, G. Xiao, A. Gupta, P. Lecoeur, J. Z. Sun, Y. Y. Wang, V. P. Dravid, *Phys. Rev. B* **1996**, *54*, R8357.
[3] S. Pignard, H. Vincent, J. P. Senateur, P. H. Giauque, *Thin Solid Films* **1999**, *347*, 161.
[4] J.-H. Kim, A. M. Grishin, H. H. Radamson, *Thin Solid Films* **2006**, *515*, 411.
[5] C. Zener, *Phys Rev.* **1951**, *81*, 440.
[6] Z. Luo, J. Gao, *Mater. Sci. Eng. B*, **2007**, *144*, 109.
[7] K.-H. Dahmen, M. Carris, *J. Alloys Comp.* **1997**, *251*, 270.
[8] L. Huang, B. Qu, L. Liu, L. Zhang, *Solid State Commun.* **2007**, *143*, 382.
[9] G. J. Snyder, R. Hiskes, S. DiCarolis, M. R. Beasley, T. H. Geballe, *Phys. Rev. B* **1996**, *53*, 14453.
[10] *Chemical Vapor Deposition: Principles and Applications* (Eds: M. L Hitchman,, K. F. Jensen) Academic Press, London, 1993.
[11] a) L. Meda, C. Bacaltchuck, H. Garmestani, K.-H. Dahmen, *J. Mater. Sci. Mater. Electronics* **2001**, *12*, 143. b) L. Meda, K.-H. Dahmen, S. Hayek, H. Garmestani, *J Cryst. Growth* **2004**, *263*, 185.
[12] a) S. Pignard, K. Y. Zhang,Y. L. Wang, K. Han, H. Vincent, J. P. Senatur, *Thin Solid Films* **2001**, *391*, 21. b) C. Duborurdieu, M-Rosina, M. Audier, E. Wiess, J. P. Senateur,E. Dooryhee, L. Hodeau, *Thin Solid Films* **2001**, *400*, 81.
[13] S. Balevicius, P. Cimmperman, V. Petrauskas,V. Stankevic, E. E. Tornau, N. Zurauskiene, A. Abrutis, V. Plausinaitiene, M. Sawicki, T. Dietl, M. Aleszkiewicz, *Thin Solid Films* **2006**, *515*, 691.
[14] X. J. Chen, H. U. Habermeier, H. Zhang, G. Gu, M. Varela, J. Santamaria, C. C. Almasan, *Phys. Rev. B.* **2005**, *72*, 104403-1.
[15] a) G. Malandrino, I. L. Fragalà, P. Scardi, *Chem. Mater.* **1998**, *10*, 3765. b) G. Malandrino, G. G. Condorelli, R. Lo Nigro, *Chem. Vap. Deposition* **2004**, *10*, 171.
[16] G. Malandrino, L. M. S. Perdicaro, G. Condorelli, I. L. Fragalà, A. Cassinese, M. Barra, *J. Mater. Chem.* **2005**, *15*, 4718.
[17] G. Malandrino, A. M. Borzì, I. L. Fragalà, A. Andreone, A. Cassinese, G. Pica, *J. Mater. Chem.* **2002**, *12*, 3728.

[18] G. Malandrino, R. Lo Nigro, I. L. Fragala, C. Benelli, *Eur. J. Inorg. Chem.* **2004,** 500.

[19] R. Lo Nigro, R. Toro, G. Malandrino, M. Bettinelli, A. Speghini, I. L. Fragalà, *Adv. Mater.* **2004**, *16*, 891.

[20] R. G. Toro, M. E. Fragalà, P. Rossi, P. Dapporto, G. Malandrino, *J. Mater. Chem.* Unpublished.

[21] D. E. Cox, T. Iglesias, E. Moshopoulou, K. Hirota, K. Takahashi, Y. Endoh, *Phys. Rev. B.* **2001**, *64*, 024431.

[22] A. Urushibara, Y. Moritomo, T. Arima, A. Asamitsu, G. Kido, Y. Tokura, *Phys. Rev. B.* **1995**, *51*, 14103.

[23] S. Mercone, C. A. Perroni, V. Cataudella, C. Adamo, M. Angeloni, C. Aruta, G. De Filippis, F. Miletto, A. Oropallo, P. Perna, A. Yu. Petrov, U. Scotti di Uccio, L. Maritato, *Phys. Rev. B.* **2005**, *71*, 064415.

[24] a) G. Malandrino, F. Castelli, I. L. Fragalà, *Inorg. Chim. Acta* **1994**, *224*, 203. b) G. Malandrino, C. Benelli, F. Castelli, I. L. Fragalà, *Chem. Mater.* **1998**, *10*, 3434.

